Conditions for the onset of plate tectonics on terrestrial planets and moons

C. O'Neill*, A.M. Jellinek† & A. Lenardic‡

Plate tectonics on Earth is driven by the subduction and stirring of dense oceanic lithosphere into the underlying mantle. For such a regime to exist on any planet, stresses associated with mantle convection must exceed the strength of the lithosphere[1,2]. That plate tectonics currently operates only on Earth indicates that this yield condition is sufficiently restrictive that mantle convection in most terrestrial planets and moons is probably in a stagnant lid regime [3,4]. Convective stresses on the lithosphere depend on the viscosity and velocity of underlying cold downwellings[2]. The lithospheric yield stress is controlled by its friction coefficient and elastic thickness (the depth to the brittle-ductile transition or BDT)[5]. Both convective stresses and the plate's yield strength depend critically on the size, thermal state and cooling history of a planet. Accordingly, here we use numerical simulations and scaling theory to identify conditions in which mantle convection leads to lithospheric failure for a range of conditions relevant to the terrestrial planets. Whereas Earth is expected to be in a plate tectonic regime over its full thermal evolution, the Moon and Mercury are expected to have always remained in a stagnant lid regime. Venus and Io currently fall on the transition between the two regimes, which is consistent with an episodic style of mantle convection for Venus[1,6] and a tectonic component to deformation on Io[7]. Our results suggest that Venus may have been in a plate tectonic regime in the past. While stagnant now, it is plausible that Mars may have also been in an active-lid regime, depending on whether there was liquid water on the surface.

Mantle convection is thought to occur in two regimes. The style of flow inferred for most terrestrial planets and moons is the "stagnant lid" regime in which mantle convection occurs beneath a strong, intact lithosphere[8,9]. Motions are expected to take the form of intermittent discrete thermals sinking from beneath the lithospheric lid and rising from the core-mantle boundary[10,11,12]. This regime is a consequence of the strong temperature-dependence of the mantle viscosity and arises because the coldest upper part of the lithosphere is too viscous to take part in the underlying flow[8,9]. In contrast, "active lid" regimes[1], which include the plate tectonic regime on the Earth, involve the foundering and stirring of cold lithosphere into the underlying mantle. Whether a planet that is initially in a stagnant lid regime can enter a plate tectonic regime depends on whether viscous stresses arising due to the formation of sinking thermals exceed the intrinsic strength of the lithosphere, which depends on temperature, water content and applied stress. The question we pose is under what conditions are

* Department of Earth Sciences, Rice University, Houston, Texas, 77030, USA (email: cjoneill@rice.edu)
† Department of Earth & Ocean Sciences, University of Britich Columbia, Vancouver, BC, Canada (email: mjellinek@eos.ubc.ca)
‡ Department of Earth Sciences, Rice University, Houston, Texas, 77030, USA (email: adrian@geophysics.rice.edu)

such convective stresses sufficient to initiate subduction? Previous work by Solomatov[13] has shown that the convective stresses for an Earth-like planet require a low lithospheric yield strength (~3MPa) to initiate subduction. Here we build on this approach by specifically considering the variations in yield strength and convective stresses over the course of a planet's thermal evolution.

A plate may permanently deform by two mechanisms; brittle failure in the cool shallow regions of the lithosphere, or by viscous flow in the hotter, deeper regions (Figure 1). The maximum supportable lithospheric stress generally occurs at the intersection of these two regimes, ie. the brittle-ductile or brittle-plastic transition[14]. Maggi et al. [5] demonstrate that the depth to which seismicity, and, by inference, brittle behaviour occurs also corresponds to the elastic lithospheric thickness. The elastic lithospheric thickness is controlled by the temperature at which significant stress-relaxation occurs over geological times; ~450°C from flexural studies on oceanic lithosphere[15,16,17], but higher for dry rheologies - and thus will scale with thermal boundary layer (ie. lid) thickness. Assuming Byerlee's frictional law[18], the maximum stress that can be accommodated without deformation is proportional to elastic thickness. Figure 1 highlights two variables which affect the BDT, the coefficient of friction μ, and the temperatures at the base of the lithosphere. Dry rock experiments[18] constrain the value of μ to be 0.6-0.85, depending on pressure, which we adopt for most planets. However, modelled deformation on Earth[19], and experiments on serpentinized rocks[20,21] suggest a much lower coefficient of friction (~0.15) for planets with liquid water on the surface (ie. Earth and maybe early Mars). The effective friction coefficient for cold ice is taken to be 0.6 [22].

Bearing in mind the complications involved in defining the BDT explicitly, for given temperature-stress-water content conditions it is appropriate to define an analog lithosphere constructed of two mechanical components: Above the BDT is the stagnant lid or "plate" component, which behaves in an essentially elastic way over the time scales for convection. Below the BDT is the "viscous" part of the cold boundary layer with thickness, δ_{vel}. Stagnant lid convection is driven by flow from the viscous region. Consequently, viscous stresses imparted to the base of the stagnant lid by this flow scale as

$$\tau = \frac{v\eta}{\delta_{vel}} \qquad \text{(Equation 1)}$$

where τ is the stress, v is a velocity scale that we discuss below, η the viscosity of the active, viscously deforming lithosphere, and δ_{vel} the velocity boundary layer thickness[17].

Our model is defined in Figure 1. Our analog plate is rigid with a viscoelastic-plastic rheology and a thickness and friction coefficient that we vary. The plate overlies a convecting mantle with a prescribed temperature, temperature-dependent viscosity law, flow geometry and velocity, v. This forced convection problem setup enables us to apply a well-defined viscous stress to the base of the plate such that we can map the conditions leading to the stability or failure of the plate in a straightforward way and over a wide range of conditions. We perform an extensive series of simulations in which we vary the

friction coefficient, the temperature at the base of the lithosphere, velocity, and mantle viscosity. Examples of plate stability and failure are shown in Figure 2.

In Figure 3 we plot the normalized driving viscous stress against the depth to the brittle-ductile transition, which is a proxy for the retarding yield stress of the plate for our suite of simulations. We identify a change in regimes, from intact to failed lithosphere, with increasing driving force or decreasing depth to the brittle-ductile transition. The dotted line demarks the transition between these two regimes, and the point where convective stresses are sufficient to overcome the plate's intrinsic strength.

Stagnant lid mantle convection in planets is not forced externally as was done in our simulations but arises naturally. Nevertheless, with an appropriate scaling for convective velocity we can apply our results to planets. The transition between intact and failing lithosphere may be understood in terms of the variation in the driving and supportable stresses with Rayleigh number (Ra). An intrinsic advantage of expressing velocity and thermal boundary thickness (δ) in terms of Ra is that the driving and retarding forces are linked to the thermal evolution of the planet. Thus, we can analyze conditions now and also project backwards in time. Solomatov & Moresi[23] show that velocity and thermal boundary layer thickness scale as $v = A\,(\kappa/d_{mantle})\,(Ra/\theta)^{\beta}$, and $\delta = (d_{mantle}/B)(\theta^{\alpha}/Ra^{\lambda})$ respectively. Here A and B are constants, $\theta = ln(\Delta\eta)$, $\Delta\eta$ is the viscosity contrast, and the exponents α, β and λ depend on the dynamics of the problem and specific rheology. Substituting these terms into Equation 1 yields an expression for the driving stress:

$$\tau_v = \left(\frac{AB}{2}\right)\frac{\eta\kappa}{d_{mantle}^{\;2}}\frac{Ra^{\beta+\lambda}}{\theta^{1+\alpha}}$$

(Equation 2)

The maximum supportable stress can be expressed as $\tau_r = \mu\rho g d_{BDT}$, and equating this and Equation 2 yields

$$\frac{d_{BDT}}{d_{mantle}} \approx \left(\frac{AB}{2C}\right)\left(\frac{\eta\kappa}{\rho g d_{mantle}^{3}}\right)\frac{Ra^{\beta+\lambda}}{\theta^{1+\alpha}}$$

(Equation 3)

For the formation of a sublithospheric drip, the relevant exponents are $\beta=\lambda=1/3$. For this case, the driving stress scales as $\tau_v \sim Ra^{2/3}$ (Equation 2), and subsequently the transition between intact and failed lithosphere (Equation 3) will scale as $Ra \sim (d_{BDT}/d_{mantle})^3$ or, alternatively, $\tau_v \sim (d_{BDT}/d_{mantle})^2$. These relationships, together with the results from our numerical simulations, are shown in Figure 3. Another appropriate scaling for the sublithospheric velocity is that for a steady laminar downwelling ($\beta=1/2$)[13,24,25,26]. The uncertainty regions in Figure 3 encapsulate the variance in applying both velocity scalings. We note that the rheology of the viscous region may be stress dependent and better described by a non-Newtonian power law such that $\varepsilon \sim \tau^n$, where $n \approx 3$ [27]. In general the effect of including such a power-law rheology is to enhance the relative velocity of downwelling drips, and hence our results are conservative in their estimate of sublithospheric velocity and driving force. A lower bound on the velocity and viscous stress for the n=3 case is an RMS mantle velocity derived numerically[27]

(β =1.21). We also include the effects of this scaling in the uncertainty regions shown.

The brittle-ductile transition for planets is calculated from estimates of their elastic lithospheric thickness (T_e), the relationship between the two is discussed in Maggi et al.[5]. T_e estimates depend strongly on the local rigidity and thermal boundary thickness, and vary considerably for a given planet. The elastic lithosphere for old oceanic lithosphere on Earth is ~40km[10,17,18]. For other planets and moons, we have adopted representative values from the literature (Table 1), and the uncertainty regions in Figure 3 include the variance in estimates of elastic thickness for these bodies.

The primary difference between the Earth and Venus, as plotted in Figure 3, is the existence of free water on the surface. This lowers the friction coefficient μ, and drastically reduces resistive strength of the lithosphere. If Venus has surface water at any time in its past, it could potentially have been in an active lid mode of convection. Even without water, increased convective velocities, and lower T_e in the past suggest that Venus may have been in active-lid regime. Its position on the transition of the stagnant-lid regime today is consistent with the recent (~750Ma) cessation of surface activity, and also permits the possibility of an episodic style of convection[1,6].

While Mars is probably in a stagnant regime now, and has been for much of its history, higher convective velocities, thinner thermal boundary layers, and the existence of surface water at 4Ga[28] potentially place Mars in the active-lid regime of Figure 3. Crustal magnetization in the Southern Highlands[29] requires the existence of a dynamo on early Mars[30], suggesting plate-tectonics in early Martian history[31,32], and our analysis suggests this is plausible. In contrast, there is no evidence of surface water on the Moon[33] or Mercury[34], and both are predicted to have been stagnant for their entire history.

The resurfacing rate of Io[7] places a constraint on interior velocities, and estimates of this plot Io on the transition between active and stagnant lid regimes, suggesting that non-volcanic surface tectonism is possible. Identification of rugged non-volcanic mountains[35] on Io indeed suggest that this deformational style is plausible. However, the stratification of tidal heating on Io is not well constrained[36], and structural styles are obscured by voluminous ongoing volcanism, and it is not clear whether an “active-lid” on Io would require a tectonic component, given the magnitude of volcanic activity. Similarly, assuming large strain-rate estimates for Europa[37] constrain interior velocities, then the surface tectonic activity observed may have an intrinsic endogenic component, separate to tidally-induced cracking[38]. In contrast, despite having a relatively small elastic lithosphere, the extremely small estimated strain rates estimated for icy shell of Ganymede[39] preclude any surface deformation other than tidally-induced tectonic features.

We have shown that the driving force required to break an intact plate is a function of the depth to the brittle-ductile transition. Exceeding this critical driving force is a necessary condition for plate tectonics on terrestrial planets, and one that is met on the Earth. Less vigorous convection and thick elastic lithospheres preclude wholesale lid failure on smaller, colder planetary bodies, such as the

Moon, Mercury, Ganymede, and present day Mars. On early Mars, more vigorous convective velocities, a thinner elastic lithosphere and the presence of free water on the surface could have resulted in plate tectonics. While the convective velocities and driving forces on Earth are intrinsically greater than for Venus, the first order difference between the two planets is surface water. Viscosity variations aside, our scalings predict that Venus may have been in an active-lid regime in the past due to increased convective velocities or if it possessed liquid water on its surface[28].

---

1. Moresi, L. & Solomatov, V., *Geophys. J. Int.***133**, 669-682 (1998).
2. Solomatov, V.S., *J. Geophys. Res.* **109,** B01412, doi:10.1029/2003JB002628 (2004)
3. Ogawa, M., Schubert, G. & Zebib, A., *J. Fluid. Mech.* **233**, 299-328 (1991).
4. Solomatov, V.S. & Moresi, L., *J. Geophys. Res.* **105**, 21795-21818 (2000).
5. Maggi, A. Jacson, J.A., McKenzie, D. & Priestley, K., *Geology* **28,** 495-498 (2000).
6. Turcotte, D.L., *J. Geophys. Res.* **98**, 17061-17068 (1993).
7. McKinnon, W.B., Schenk, P.M. & Dombard, A.J. *Geology* **29**, 103-106 (2000).
8. Moresi, L. & Solomatov, V.S., *Phys. Fluids*. **7**, 2154-2162 (1995).
9. Solomatov, V.S. & Moresi, L. *Geophys. Res. Lett.* **24**, 1907-1910 (1997).
10. Jellinek, A.M. & Manga, M. *Rev. Geophys.* **42**, RG3002, doi:10.1029/2003RG000144 (2004).
11. Jellinek, A.M., Lenardic, A. & Manga, M. *Geophys. Res. Lett.* **29**, 1532, doi: 10.1029/2001GL014624 (2002).
12. Manga, M.D., Weeraratne, D. & Morris, S.J.S. *Phys Fluids* **13**, 802-805 (2001).
13. Solomatov, V.S. *J. Geophys. Res.* **109**, B01412, doi:10.1029/2003JB002628 (2004).
14. Kohlstedt, D.L., Evans, B. & Mackwell, S.J. *J. Geophys. Res.* **100**, 17587-17602 (1995).
15. Watts, A.B. & Burov, E.B. *Earth Planet. Sci. Lett.* **213**, 113-131 (2003).
16. Turcotte, D.L. & Schubert, G. *Geodynamics* (Cambridge University Press, Cambridge, New York, 2002).
17. Calmant, S., Francheteau, J. & Cazenave, A. *Geophys. J. Int.* **100**, 59-67 (1990).
18. Byerlee, J.D. *J. Geophys. Res*. **73**, 4741-4750 (1968).
19. Beaumont, C. Muñoz, J.A., Hamilton, J. & Fullsack, P. *J. Geophys. Res.* **105**, 8121-8145 (2000).
20. Escartin, J. Hirth, G. & Evans, B. *Geology* **29**, 10223-1026 (2001
21. Escartin, J. Hirth, G. & Evans, B. *Earth Planet. Sci. Lett.* **151**, 181-189 (1997).
22. Beeman, M., Durham, W.B. & Kirby, S.H. *J. Geophys. Res.* **93**, 7625–7633 (1988).

23. Solomatov, V.S. & Moresi, L. *J. Geophys. Res.* **105**, 21795-21817 (2000).
24. Batchelor, G.K. *Q. J. R. Met. Soc.* **80**, 339-359 (1954).
25. Worster, M.G. & Leitch, A.M. *J. Fluid Mech*. **156**, 301-319 (1985).
26. Kaminski, E. & Jaupart, C. *J. Fluid. Mech.* **478**, 287-298 (2003).
27. Reese, C.C., Solomatov, V.S. & Moresi, L. *J. Geophy. Res.* **103**, 13643-13658 (1998).
28. Catling, D.C., *Nature* **429**, 707-708 (2004).
29. Acuna, M.H., et al. *Science* **284**, 790-793 (1999).
30. Nimmo F. & Stevenson, D.J. *J. Geophys. Res.* **105**, 11969-11979 (2000).
31. Sleep, N. H. *J. Geophys. Res.* **99**, 5639-5655 (1994).
32. Lenardic, A. Nimmo, F. & Moresi, L. *J. Geophys. Res.* **109**, E02003, doi: 10.1029/2003JE002172 (2004).
33. Lissauer, J.J. *Nature*, **389**, 327-328 (1997).
34. Lewis, J.S. in *Mercury* (ed. F. Vilas, et al.), Univ. Ariz. Press, Tuscon, Az. 651-666 (1988).
35. Carr, M.H. et al. *Icarus*, **135**, 146-165 (1998).
36. Moore, W.B. *J. Geophy. Res.* **108**, doi: 10.1029/2002JE001943 (2003).
37. Ojakangas, G.W. & Stevenson, D.J. *Icarus*, **81**, 220-241 (1989).
38. Nimmo, F. & Gaidos, E. *J. Geophys. Res.* **107**, doi: 10.1029/2000JE1476 (2002).
39. Dombard, A.J. & McKinnon, W.B. *Icarus* **154**, 321-336 (2001).

Acknowledgements
This work was supported by NASA-MDAT grant NAG5-12166 & NSF Grant EAR-0448871. MJ acknowledges the assistance of the NSERC and The Canadian Institute for Advanced Research.

Figure Captions

Figure 1. (a) Deformation mechanisms within a cold lid with a viscoelastic-plastic rheology. At low stress and temperature (T), the lid behaves elastically. Once the stress exceeds the yield stress of the lithosphere, the lid fails and behaves in a brittle manner. The criteria for yielding is defined by Byerlees' law[18] $\tau_{yield} = C_0 + \mu P$, where Co is the cohesion, μ the coefficient of friction, and P the pressure. At higher temperatures, the lid behaves viscously, where the viscosity is defined by a temperature-dependent law $\eta_{lid} = \frac{b}{\tau^{n-1}} e^{-\gamma T}$, where n=1 corresponds to a Newtonian fluid, n>1 is for a power-law rheology, and b and γ are constants[23]. The maximum supportable lithospheric stress occurs at the brittle-ductile transition (BDT), ie. the intersection of the latter two deformational styles. The depth of this transition depends on both μ and the mantle temperatureT_m.
(b) Experimental setup for our numerical simulations. We impose a strong lid of thickness d. The mantle beneath the lid is at a constant T_m, with a viscosity η_m, and is stirred by two conveyor belts turning at a velocity V_m, which we vary. The convective stress imparted on the lid is a function of the velocity of the active downwelling (blue), generally V_m in our simulations.

(c) Sub-lithospheric velocities due to cold-downwellings, either in the form of a sinking drip (left) or steady flow into a conduit (right[26]).

Figure 2. Numerical simulation of failing lithosphere (**a**, left) and stable lithosphere (**b**, right). The viscoelastic-plastic lid is shaded dark blue, the viscous mantle aqua. Areas undergoing plastic deformation are shaded translucent red regions, and the velocity field is shown as arrows. All our simulations were performed using Ellipsis (see Moresi & Solomatov[1] for details), which solves the standard convective equations[1] for the experimental setup shown in Figure 1. The simulations are non-dimensionalized in the manner of Moresi & Solomatov[1], assuming appropriate distance (d_0), viscosity (η_0), temperature (ΔT) and velocity (κ/d_0) scales (subscript denotes reference value). The initial depth to the BDT in both cases is 0.08, and the coefficient of friction μ is 0.2. Both examples use a mantle viscosity of 1, a T_m of 100, and a lid thickness of 0.12. The imposed velocity (V_m) in **(a)** is 200, while for **(b)** its 10. As a consequence of the large driving force in **(a)**, relative to the lid's resistive strength, the lid fails and is eventually recycled into the mantle. In contrast the driving force in **(b)** is insufficient to overcome the strength of the lid, and the lid remains intact.

Figure 3. Log-linear plot of the variation in tectonic style with increasing driving force and depth to the brittle-ductile transition (BDT). The results are non-dimensionalised by dividing the BDT by the depth of the convecting layer d, and by dividing the driving velocity and mantle viscosity by (κ/d) and η_0 respectively, and combining the two to give the upper thermal boundary layer stress (Equation 1). The results of our numerical experiments are shown depending on their deformational response; blue squares indicate intact lithosphere, and red diamonds indicate failed lithosphere. The transition between the two regimes is plotted as a dashed line. Planets and satellites for which reliable estimates of mantle depth, elastic lithospheric thickness and mantle velocity exist (Table 1) are also nondimensionalized and plotted. Driving forces at 4.5Ga are determined assuming higher internal heat production and Rayleigh numbers (see Table 1). The coefficient of friction is assumed to be 0.6 for dry rock and ice[18,22], and 0.15 for rocky planets with free water on the surface (Earth and early Mars, Escartin et al.[20,21]). Coloured regions indicate the uncertainty in our estimates, based on the listed uncertainties in the elastic lithospheric thickness (Table 1), and the variance in the velocity scalings. **(a)** Linear plot of Fdrive/μ vs BDT/d. Results of our simulations are also plotted. The transition between failed and intact lithosphere follows the relationship $F_{drive} \sim (BDT/d)^2$ for this n=1 case. **(b)** Log-log plot of Ra vs (BDT/d)μ. Calculation of Ra assumes the drip scaling discussed in the text. The transition between failed and intact lithosphere behaves as $Ra \sim (\mu BDT/d)^3$ for the n=1 case.

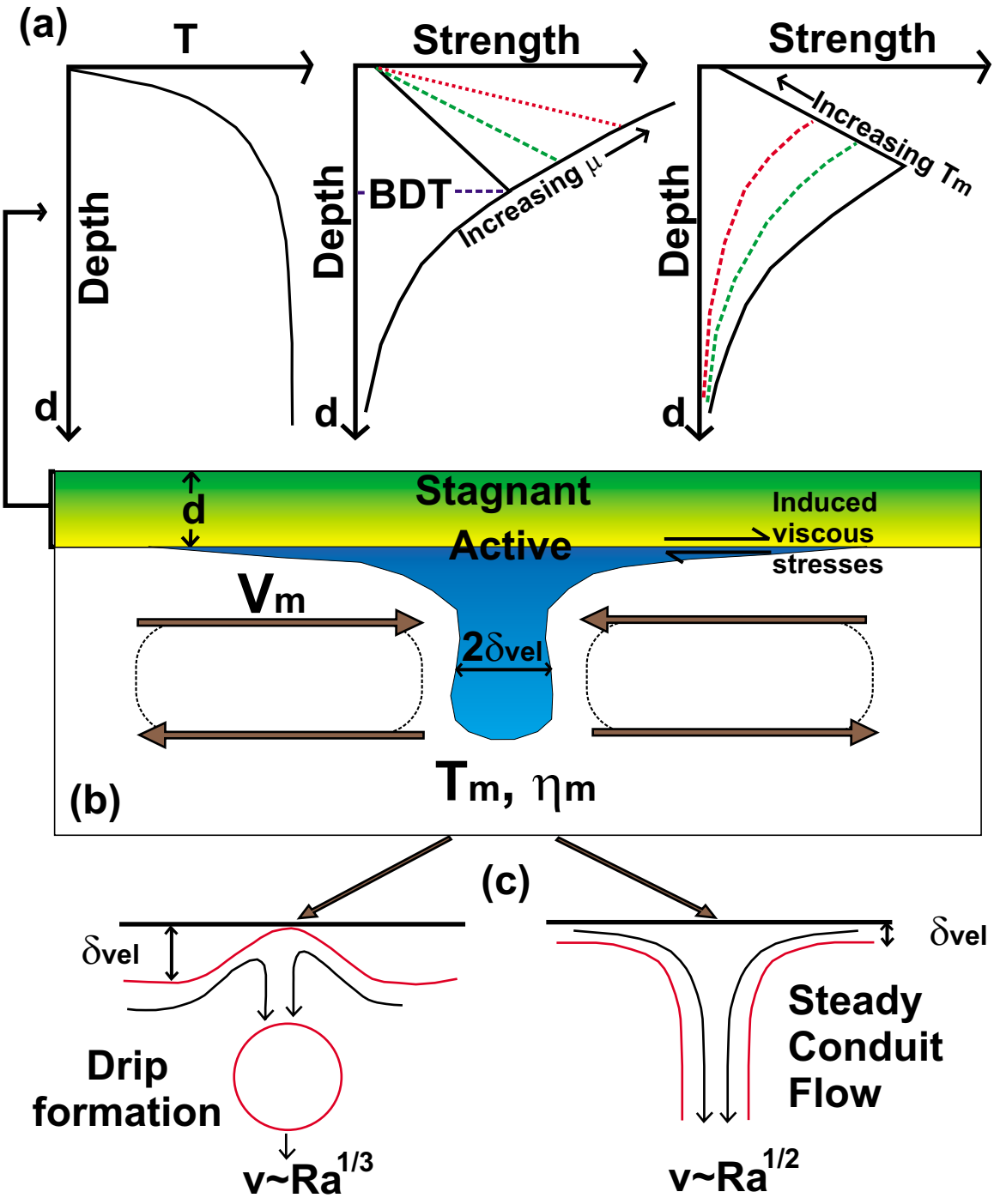
(a)
T
Depth
d
Strength
Depth
BDT
Increasing μ
d
Strength
Increasing Tm
Depth
d
d
Stagnant
Active
Induced
viscous
stresses
Vm
2δvel
Tm, ηm
(b)
(c)
δvel
Drip
formation
v~Ra1/3
δvel
Steady
Conduit
Flow
v~Ra1/2

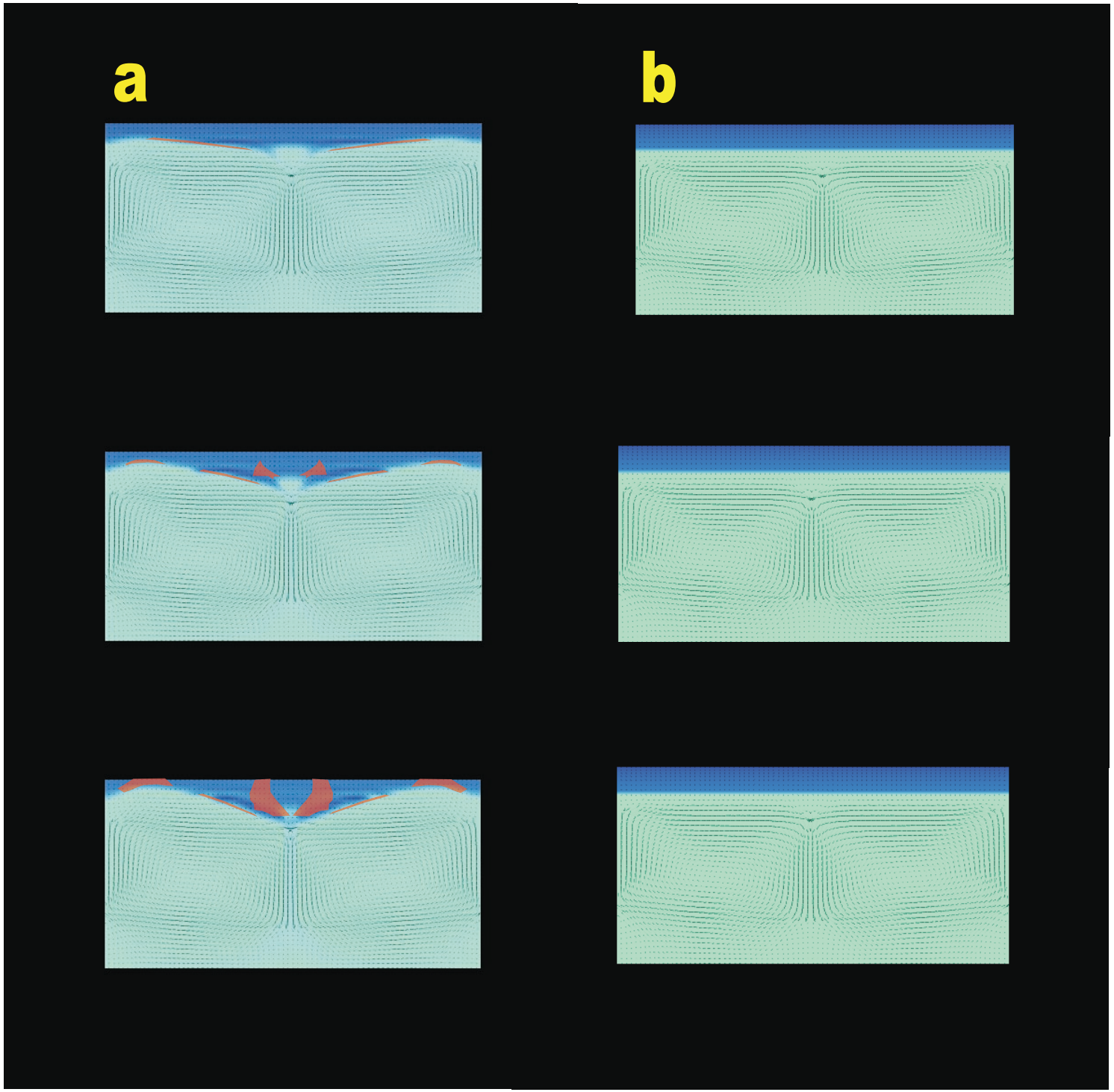
a
b

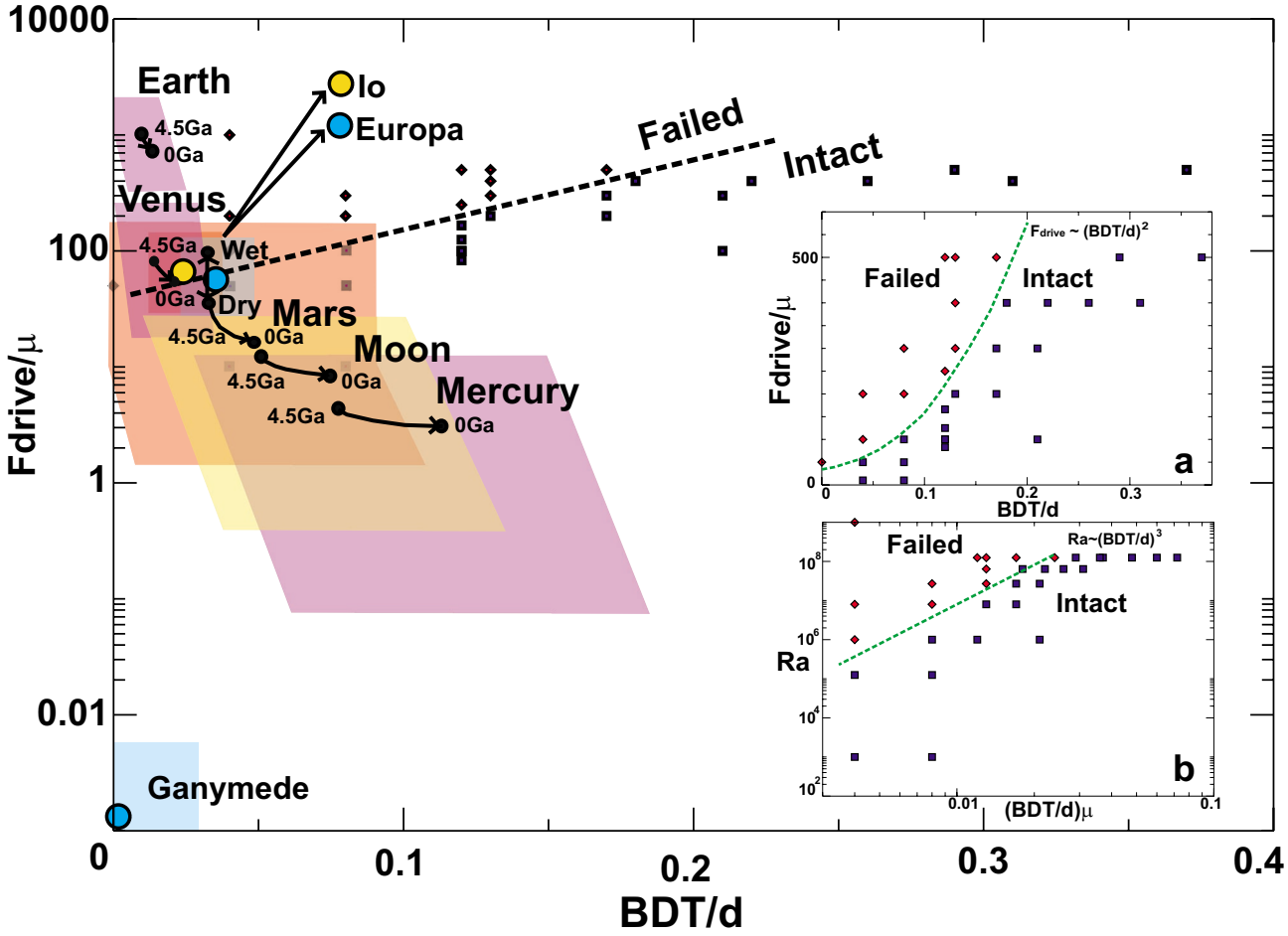
Earth
Io
Europa
Failed
Intact
Venus
4.5Ga
0Ga
Wet
Dry
Mars
Moon
Mercury
Ganymede
Fdrive/μ
BDT/d
10000
100
1
0.01
0
0.1
0.2
0.3
0.4
Fdrive ~ (BDT/d)²
Failed
Intact
a
Ra~(BDT/d)³
Ra
(BDT/d)μ
b